Nanoscale Advances

ROYAL SOCIETY OF CHEMISTRY

PAPER

View Article Online
View Journal | View Issue

Cite this: *Nanoscale Adv.*, 2020, **2**, 3027

Key factors affecting Rayleigh instability of ultrathin 4H hexagonal gold nanoribbons†

Peifeng Li, *[a] Weibing Liao,[b] Lijie Yue,[c] Zhanxi Fan *[de] and Feng Rao*[a]

Received 5th March 2020
Accepted 22nd May 2020

DOI: 10.1039/d0na00186d

rsc.li/nanoscale-advances

Rayleigh instability was originally used to describe the phenomenon of a cylindrical fluid jet that transforms into a chain of droplets. Very recently, it has been extended to metallic nanostructures like gold (Au) and silver (Ag) nanowires (NWs), as well as mixed alloy NWs by some thermodynamic processes. To date, the key factors affecting the Rayleigh instability have not been well studied. To clarify this, we systematically investigate the features of Rayleigh instability in ultrathin 4H hexagonal Au nanoribbons (NRBs) under electron beam (E-beam) irradiation. We prove that by decreasing the initial widths of 4H Au NRBs and the E-beam current density, as well as the irradiation time and intensity per unit area, the Rayleigh instability can be effectively restrained. Our work thus sheds light on how to effectively reduce or even eliminate the Rayleigh instability of one dimensional nanomaterials.

Introduction

Since the last decade, the unique physical and chemical properties of ultrathin gold nanowires (Au NWs) with less than 10 nm in diameter have been well-studied,[1–4] opening up a new era for the synthesis and application of one dimensional (1D) ultrathin metallic nanostructures.[5–9] In particular, ultrathin Au nanostructures hold great promise for application in next-generation nanoelectronics and metal interconnection,[10–13] owing to their intriguing electrical and mechanical properties, as well as the desired chemical inertness.[14–16] However, such ultrathin Au nanostructures, for instance NWs upon heating, usually undergo microstructural changes to different extents and will finally be shattered into chains of nanospheres due to Rayleigh instability,[17–19] during the observation, characterization or welding under electron beam (E-beam) irradiation.[19–22] The wrinkling phenomenon of Rayleigh instability, revealed by first-principles calculations and continuum mechanics, is caused by the anisotropy in the surface stresses and in the elastic response.[20] From *in situ* high resolution transmission electron microscope (HRTEM) observations, the underlying mechanism of such anisotropy is proved to be the mass transport driven by surface atom migration.[21] Under ~500–700 °C, the Rayleigh instability is even more severe that the Au nanoribbons (NRBs) break more easily and change into a chain of nanospheres, and the substrate-supported Au NRBs transform into irregular nanoparticles.[22] For the new exotic metastable 4H hexagonal ultrathin Au NRBs,[23–25] the Rayleigh instability occurs upon E-beam irradiation with the heating temperature below 400 K, but the 4H phase remains stable.[26] Although the Rayleigh instability of 1D metallic nanostructures has long been known, its key influencing factors have not been well studied.

It has been well-documented that the geometric shape changes of nanomaterials will result in significant variations in the electronic structure, electrical transport characteristics, and energy dissipation level.[27] To alleviate the negative effect of Rayleigh instability on the geometric shapes and physical properties of Au nanostructures, the influencing factors need to be systematically studied. For this purpose, in this work, *in situ* TEM E-beam irradiation was employed to induce Rayleigh instability of ultrathin 4H Au NRBs. We reveal that the Rayleigh instability can be suppressed by adjusting the initial widths of 4H Au NRBs and modulating the parameters of E-beam irradiation as well.

Results and discussion

The 4H Au NRBs were synthesized according to a previously reported method.[23] Fig. 1a shows the typical TEM images of Au NRBs with a uniform size and smooth surface. The HRTEM image and corresponding fast Fourier transform (FFT) pattern in Fig. 1b demonstrate the good crystallinity and unconventional 4H hexagonal phase of the as-prepared Au NRBs. Another two samples have folding/kink parts as shown in Fig. S1† which reveals their NRB shape.

[a]*College of Materials Science and Engineering, Shenzhen University, Shenzhen 518060, China. E-mail: peifengli@szu.edu.cn; fengrao@szu.edu.cn*

[b]*College of Physics and Energy, Shenzhen University, Shenzhen 518060, China*

[c]*School of Materials Science and Engineering, Shandong University of Science and Technology, Qingdao 266590, China*

[d]*Department of Chemistry, City University of Hong Kong, Kowloon 999077, Hong Kong, China. E-mail: zhanxi.fan@cityu.edu.hk*

[e]*Hong Kong Branch of National Precious Metals Material Engineering Research Center (NPMM), City University of Hong Kong, Hong Kong, China*

† Electronic supplementary information (ESI) available. See DOI: 10.1039/d0na00186d

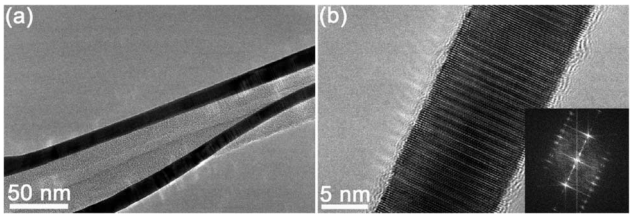

Fig. 1 TEM images of 4H Au NRBs: (a) low magnification TEM image, and (b) HRTEM image and the corresponding FFT pattern (inset).

Rayleigh instability of 4H Au NRBs

An ultrathin 4H Au NRB (sample 1) with an initial width (w) of 10.9 nm was irradiated using E-beam with a constant current density of ~50 pA cm^{-2} in a TEM machine (JEM-2100F). Fig. 2 shows its evolution process with time under E-beam irradiation. Before the irradiation, the Au NRB is straight and flat (Fig. 2a). After 10 min of irradiation, Rayleigh instability occurred with ripples formed at the edges (Fig. 2b). From 10 to 50 min, the shape evolution became more and more obvious, and the ripples grew into approximately symmetrical sine gradients (Fig. 2c–f). More detailed information can be found in Movie S1† (0–10 min) and Movie S2† (45–50 min).

The 3D schematics of the Au NRB with different views before and after Rayleigh instability are shown in Fig. 3a and b. The dimensional changes after Rayleigh instability can be characterized through three parameters in the normal view of Fig. 3b, *i.e.* the peak width (w_p), trough width (w_t), and mid width (w_m, *i.e.* the width of the site in the middle of the peak and trough). The changes of these three widths along with the irradiation time can be measured by *in situ* TEM. By taking the 50 min E-beam irradiation point as an example (Fig. 2f), these three widths were found to be as follows, *i.e.* w_p = 10.3 nm, w_t = 5.7 nm and w_m = 8.3 nm. More detailed information at other times can be found in Table S1 in the ESI.† As a result, the peak widths (pink line), trough widths (violet line) and mid widths (red line) as a function of time can be obtained, as shown in Fig. 3c. All the widths show approximately a linear decrease with irradiation time.

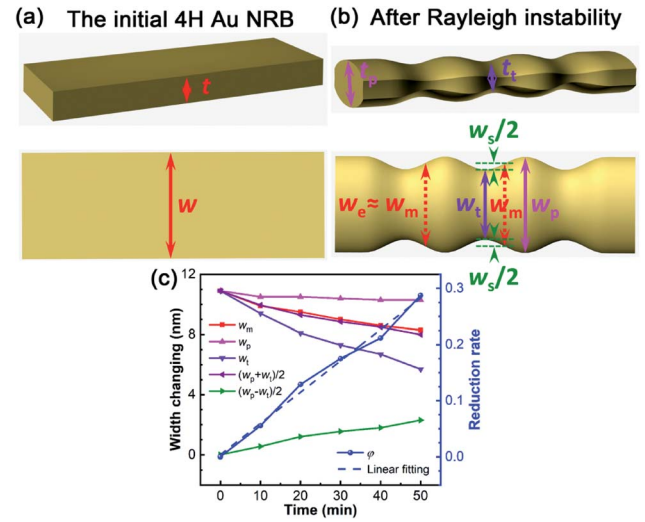

Fig. 3 (a) 3D schematics of the 4H Au NRB before and (b) after Rayleigh instability occurred. (c) Relationships between the mid width, peak width, trough width, average/effective width, shrinking width, width reduction rate and irradiation time.

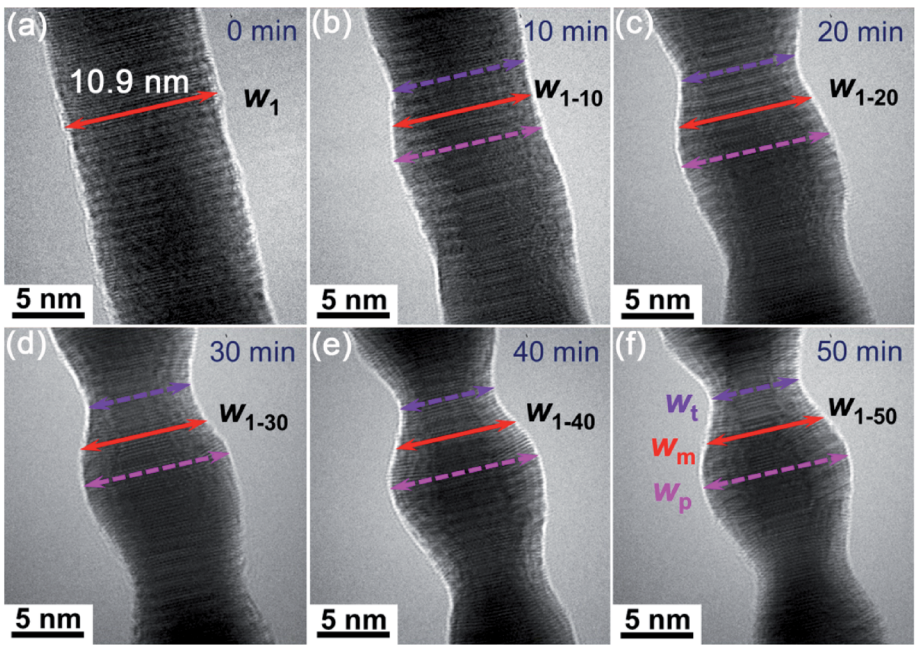

Fig. 2 Evolution processes of the Rayleigh instability occurring in a 4H Au NRB with a width of 10.9 nm: before (a) and after E-beam irradiation for (b) 10 min, (c) 20 min, (d) 30 min, (e) 40 min, and (f) 50 min, respectively. The red solid arrows represent the mid width changes of the 4H Au NRB after E-beam irradiation for different times, while the pink and violet dashed arrows represent the peak and trough width changes as the irradiation time increased.

It is worth noting that the peak width of ultrathin 4H Au NRBs after E-beam irradiation was smaller than their initial width (w), which is different from the case of Au NWs.[21] The schematic diagrams in Fig. 3a and b also reveal the size changes before and after Rayleigh instability. In most cases, both the peak width and trough width of Au NRBs decreased in the evolution process. According to the principle of constant volume, both the peak thickness (t_p) and trough thickness (t_t) increased during the evolution process. However, t_t would decrease after exceeding a certain time of E-beam irradiation. The width reduction and thickness increase are supposed to decrease the surface energy in the evolution process, which is consistent with the phenomenon observed in our previous study.[26]

Evolution process of Rayleigh instability

In order to further quantify the degree of Rayleigh instability, it is necessary to define the effective width (w_e) and shrinking width (w_s) of 4H Au NRBs that are shown in Fig. 3b. w_e is approximately equal to w_m and the average width (w_a), as calculated using the following equation:

$$w_e \approx w_m \approx w_a = \frac{(w_p + w_t)}{2}. \quad (1)$$

w_s can be calculated using the following equation:

$$w_s = w_e - w_t \approx \frac{(w_p + w_t)}{2} - w_t = \frac{(w_p - w_t)}{2}. \quad (2)$$

The effective widths and shrinking widths at different times can be measured from the TEM images, as shown in Table S1.† The curves of width change along with time can thus be obtained (Fig. 3c). As the irradiation time increased, the effective widths (purple line) decreased, while the shrinking widths (green line) increased gradually. Because the mid width curve is almost overlapped with the average width curve, the average widths can be replaced by the mid widths in the case of low accuracy requirements (*i.e.* $w_e \approx w_a \approx w_m$).

The evolution degree of the Rayleigh instability can be described using the width reduction rate (φ), which can be calculated using the following equation.

$$\varphi = \frac{w_s}{w_e} = \frac{(w_p - w_t)/2}{(w_p + w_t)/2} = \frac{(w_p - w_t)}{(w_p + w_t)}. \quad (3)$$

As a result, the width reduction rates of 4H Au NRBs at different irradiation times can be calculated using eqn (3), as shown in Table S1.† The relationship between width reduction rates and the irradiation time is demonstrated in Fig. 3c (*i.e.* the blue curve). Note that the fitted slope of the linear fitting curve is about 0.00558. The width reduction rate has an approximate linear relationship with the irradiation time, indicating that the evolution degree of Rayleigh instability increases linearly as the irradiation time is extended. Thus, in order to reduce the evolution degree of Rayleigh instability in Au NRBs, one should reduce the irradiation time.

According to the shape and size changes of 4H Au NRBs under E-beam irradiation, the atom migration paths can be speculated. At the trough sites, the Au atoms first migrate in the inner radial direction of Au NRBs, then along the longitudinal direction pointing to the peak sites, and finally in the outer radial direction pointing to the peak sites. The atom migration path is shown in Fig. S2† with violet arrow 1 (the density of the color represents the atom migration density; only one path is depicted, and other symmetric paths are omitted). At the peak sites, the atoms mainly migrate in the inner radial direction of the Au NRB, as shown in Fig. S2† with pink arrow 3. At the mid sites, the atoms migrate along path 1, with a weakened migration degree, as in Fig. S2† with red arrow 2. The atom migration paths at other sites can be combined by the above three paths. Fig. S2† also shows the traces left by atom migration during the evolution process marked with sinusoidal orange curves. The parallel ripple curves between the edges and the sinusoidal orange curves denote the borders of different atomic layers. The migration of ripple curves can be clearly seen in Movie S2.† Furthermore, the atoms migrate in the thickness direction at the same time so as to decrease the surface energy of the Au NRB in the evolution process, leading to the increase of its thickness.[26]

Another significant difference between NWs and NRBs during the evolution process is the wavelength (λ, *i.e.* peak to peak or trough to trough) of the sinusoidal shape. For the NWs, the minimum wavelength (λ_{min}) is $2\pi R_0$ after Rayleigh instability.[19] Thus the minimum ratio of the wavelength to diameter is π (*i.e.* $r_{min} = \lambda/d = \lambda_{min}/2R_0 = \pi$). For sample 1, the wavelength is 12.9 nm, which can be measured from Fig. S2† (the yellow arrow between trough to trough). The ratios of the wavelength to effective width (λ/w_e) at 10, 30 and 50 min are calculated as follows:

$$r_{10} = \lambda/w_{e-10} = \frac{12.9}{9.95} = 1.30, \quad r_{30} = \lambda/w_{e-30} = \frac{12.9}{8.85} = 1.46,$$
$$r_{50} = \lambda/w_{e-50} = \frac{12.9}{8.0} = 1.61.$$

The λ/w_e ratios in the NRB are considerably smaller than the λ/d ratio in the NW.[19] This is mainly attributed to the high ratio of the width to thickness in the NRB, which leads to a much larger effective width compared to the diameter of the NW. However, the λ/w_e ratios increase almost linearly due to the effective width reduction with time (Fig. S2b†). With enough irradiation time, when the cross section of the NRB changes from rectangular to circular completelyy, the ratio would reach the maximum value.

Factors affecting the Rayleigh instability

To further reveal the size effect on the Rayleigh instability of ultrathin 4H Au NRBs, another three Au NRBs (*i.e.* samples 2–4) with different initial widths were chosen to be investigated at a lower irradiation intensity per unit area (low magnification) as compared to sample 1 (high magnification). Fig. 4a, c and e show TEM images of the three NRBs with initial widths of 14.5 nm (w_2), 9.6 nm (w_3) and 11.8 nm (w_4), respectively. Their

morphologies after 20, 30, and 40 min of irradiation are shown in Fig. 4b, d and f. The detailed information of their size evolution is shown in Table S2 in the ESI† with a black font. According to the linear relationship between the width reduction rate and irradiation time, the size evolution at other times can be deduced, as shown in Table S2† with a red font. Then, using eqn (1)–(3), the width reduction rates of the three Au NRBs at 20 min and other corresponding detailed information of size evolution were calculated and are shown in Table S3 in the ESI.† Fig. 4g shows the relationship between the width reduction rates of Au NRBs and their initial widths after 20 min of E-beam irradiation. The exponential fitting is drawn and shown with orange dashed lines (the exponential equation is shown as eqn (S1) in the ESI†). The results reveal that the width reduction rates of Au NRBs increased almost exponentially as their initial widths increased. In other words, the ultrathin Au NRBs with a smaller initial width have higher resistance to Rayleigh instability.

We have proved that a higher E-beam current density shall accelerate the evolution process of Rayleigh instability.[24] Therefore, the effect of irradiation intensity per unit area on the Rayleigh instability is also explored here. This is mainly from the perspective of energy.[28] It is worth noting that the most likely cause of Rayleigh instability is Joule heat induced by E-beam irradiation which has been discussed in our previous research studies.[21,26] The Joule heat comes from the kinetic energy ($E_k = eU = 1/2mv^2$, U: the accelerating voltage) consumption of the accelerating electrons in the collision process with the 4H ultrathin Au NRBs. We can approximate that the amount of Joule heat is proportional to the accelerating voltage. The rest is taken away by the slowing electrons reflected by the 4H ultrathin Au NRBs. Actually, in order to investigate the effect of the accelerating voltage (energy or Joule heat essentially) on the evolution rate in the Rayleigh instability process, we consider another parameter "irradiation intensity per unit area" to characterize. The high and low irradiation intensity per unit area is presented by the observation magnification. The higher the observation magnification is, the more electron collisions or Joule heat is generated in per unit area in the 4H ultrathin Au NRBs. Using eqn (S1),† the equivalent width reduction rate (φ_l) of sample 1 with a width of 10.9 nm at 20 min with a low irradiation intensity per unit area can be obtained

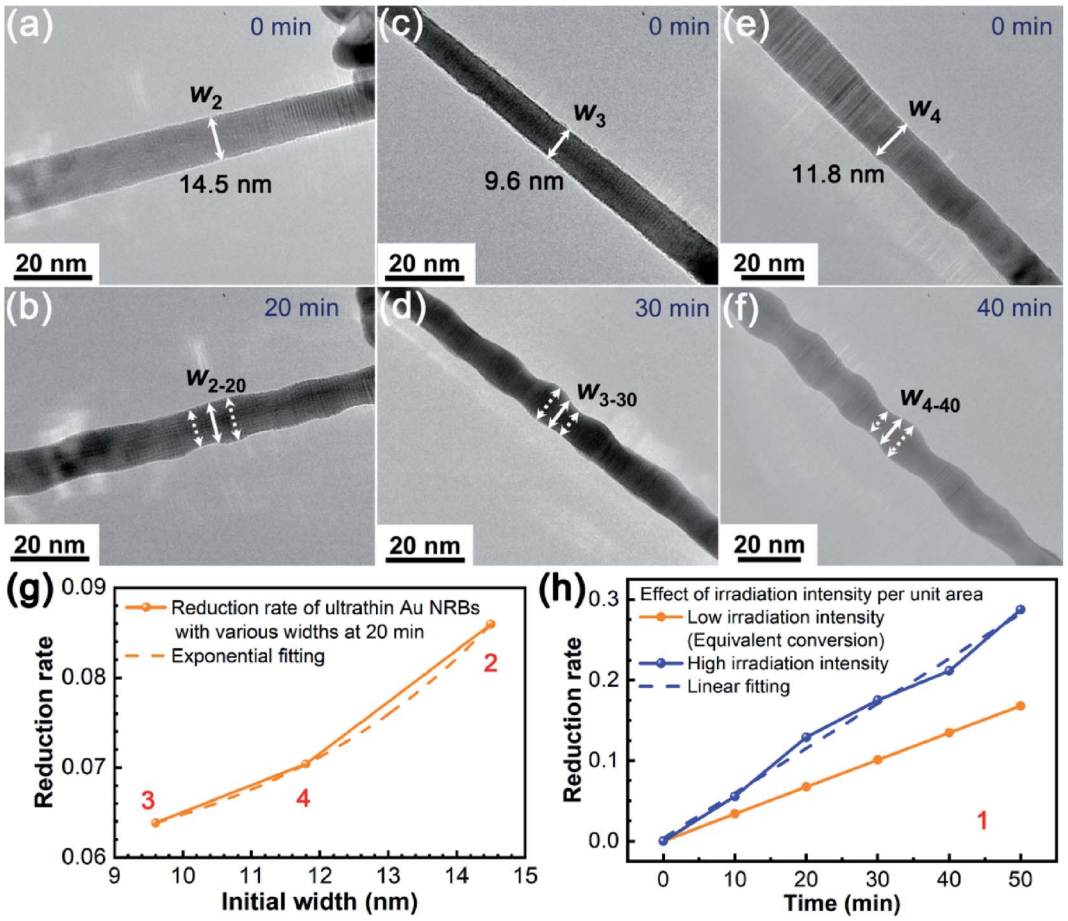

Fig. 4 Size effect on Rayleigh instability of 4H Au NRBs with various initial widths of (a) 14.5 nm, (c) 9.6 nm, and (e) 11.8 nm under E-beam irradiation for (b) 20 min, (d) 30 min, and (f) 40 min, respectively. (g) Relationships between width reduction rates and initial widths. (h) The width reduction rate increased as the irradiation intensity per unit area increased. The blue line at a high irradiation intensity per unit area represents the experimental data, while the orange line at a low irradiation intensity per unit area represents the equivalent conversion curve. The digits 1–4 in (g and h) denote the sample serial numbers.

(*i.e.* 0.067236). Then, according to the linear relationship between width reduction rates and the irradiation time, the equivalent width reduction rates of sample 1 at other times can be determined using eqn (S2) in the ESI.† The equivalent width reduction rate values (φ_1) are shown in Table S1.† The relationship curve between equivalent width reduction rates and the irradiation time is shown in Fig. 4h (orange line). The experimental relationship curve obtained in Fig. 3c is also shown in Fig. 4h (blue line) for comparison. The ratio of their slopes ($R = s_h/s_l = 0.00558/0.0033618 = 1.66$) indicates the enhancement of the Rayleigh instability with a high irradiation intensity per unit area. The results revealed that the lower irradiation intensity per unit area has smaller influence on the Rayleigh instability.

Conclusions

In summary, the evolution processes and degrees of Rayleigh instability in ultrathin 4H Au NRBs under *in situ* E-beam irradiation were characterized systematically. The influencing factors of Rayleigh instability were also investigated. Both the trough and peak widths of Au NRBs shrunk during the evolution process due to the atom migration in the thickness direction. In addition, at the peak sites of the sinusoidal shape, the atoms migrated from the edges in their inner radial direction, while at other sites the atoms also migrated to the peak sites along the longitudinal direction. The evolution degree of the Rayleigh instability can be characterized by the width reduction rates of Au NRBs. The width reduction rates of Au NRBs increased as their initial widths, irradiation time, irradiation intensity per unit area and E-beam current density increased. The research results provide us some methods to prevent or reduce Rayleigh instability of 4H Au NRBs or other ultrathin nanostructures through controlling the above four influencing factors.

Experimental section

The ultrathin 4H Au NRBs were synthesized by a chemical method that was described in detail in the previous work.[23] The characteristics, evolution processes and influencing factors of Rayleigh instability in ultrathin Au NRBs were investigated by means of *in situ* TEM.[14] All the *in situ* experiments were performed in a JEOL JEM-2100F TEM with a voltage of 200 kV. The ultrathin 4H Au NRBs with various initial widths were irradiated using E-beam with a constant current density value of ~50 pA cm^{-2} for different times.

Conflicts of interest

The authors declare no competing financial interest.

Acknowledgements

The authors acknowledge the financial support from the Natural Science Foundation of Guangdong Province, China (2018A030313793). Peifeng Li also thanks Dr Zengze Wang for drawing the 3D images of the Au NRBs before and after Rayleigh instability. Zhanxi Fan acknowledges the support from ITC *via* the Hong Kong Branch of National Precious Metals Material Engineering Research Center (NPMM), and the Start-Up Grant (Project No. 9610480 and 7200651) support from the City University of Hong Kong.

References

1 A. Halder and N. Ravishankar, Ultrafine single-crystalline gold nanowire arrays by oriented attachment, *Adv. Mater.*, 2007, **19**, 1854–1858.
2 C. Wang, Y. Hu, C. M. Lieber and S. Sun, Ultrathin Au nanowires and their transport properties, *J. Am. Chem. Soc.*, 2008, **130**, 8902–8903.
3 X. Lu, M. S. Yavuz, H. Tuan, B. A. Kogel and Y. Xia, Ultrathin gold nanowires can be obtained by reducing polymeric strands of oleylamine-AuCl complexes formed *via* aurophilic interaction, *J. Am. Chem. Soc.*, 2008, **130**, 8900–8901.
4 Z. Huo, C. Tsung, W. Huang, X. Zhang and P. Yang, Sub-two nanometer single crystal Au nanowires, *Nano Lett.*, 2008, **8**, 2041–2044.
5 L. Cademartiri and G. A. Ozin, Ultrathin nanowires-A materials chemistry perspective, *Adv. Mater.*, 2009, **21**, 1013–1020.
6 Y. Wang, S. I. Choi, X. Zhao, S. Xie, Y. Xia, *et al.*, Polyol synthesis of ultrathin Pd nanowires *via* attachment-based growth and their enhanced activity towards formic acid oxidation, *Adv. Funct. Mater.*, 2014, **24**, 131–139.
7 D. Wen, S. Guo, S. Dong and E. Wang, Ultrathin Pd nanowire as a highly active electrode material for sensitive and selective detection of ascorbic acid, *Biosens. Bioelectron.*, 2010, **26**, 1056–1061.
8 L. Ruan, E. Zhu, Y. Chen, Z. Lin, Y. Huang, *et al.*, Biomimetic synthesis of an ultrathin platinum nanowire network with a high twin density for enhanced electrocatalytic activity and durability, *Angew. Chem., Int. Ed.*, 2013, **52**, 1–6.
9 B. Y. Xia, H. B. Wu, Y. Yan, X. W. Lou and X. Wang, Ultrathin and ultralong single-crystal platinum nanowire assemblies with highly stable electrocatalytic activity, *J. Am. Chem. Soc.*, 2013, **135**, 9480–9485.
10 U. Chandni, P. Kundu, S. Kundu, N. Ravishankar and A. Ghosh, Tunability of electronic states in ultrathin gold nanowires, *Adv. Mater.*, 2013, **25**, 2486–2491.
11 S. Pud, A. Kisner, M. Heggen, D. Belaineh, S. Vitusevich, *et al.*, Features of transport in ultrathin gold nanowire structures, *Small*, 2013, **9**, 846–852.
12 A. Roy, T. Pandey, N. Ravishankar and A. K. Singh, Single crystalline ultrathin gold nanowires: promising nanoscale interconnects, *AIP Adv.*, 2013, **3**, 032131.
13 C. Schirm, M. Matt, F. Pauly, J. C. Cuevas, E. Scheer, *et al.*, A current-driven single-atom memory, *Nat. Nanotechnol.*, 2013, **8**, 645–648.
14 K. Critchley, B. P. Khanal, M. L. Gorzny, L. Vigderman, N. A. Kotov, *et al.*, Near-bulk conductivity of gold nanowires as nanoscale interconnects and the role of

atomically smooth interface, *Adv. Mater.*, 2010, **22**, 2338–2342.

15 Y. Lu, J. Y. Huang, C. Wang, S. Sun and J. Lou, Cold welding of ultrathin gold nanowires, *Nat. Nanotechnol.*, 2010, **5**, 218–224.

16 Y. Lu, J. Song, J. Y. Huang and J. Lou, Fracture of sub-20 nm ultrathin gold nanowires, *Adv. Funct. Mater.*, 2011, **21**, 3982–3989.

17 L. Rayleigh, On the instability of jets, *Proc. Lond. Math. Soc.*, 1878, **10**, 4–13.

18 L. Rayleigh, On the instability of cylindrical fluid surfaces, *Phil. Mag.*, 1892, **34**, 177–180.

19 S. Karim, M. E. Toimil-Molares, A. G. Balogh, W. Ensinger, T. W. Cornelius, *et al.*, Morphological evolution of Au nanowires controlled by Rayleigh instability, *Nanotechnology*, 2006, **17**, 5954–5959.

20 A. Roy, S. Kundu, K. Müller, A. Rosenauer, A. K. Singh, *et al.*, Wrinkling of atomic planes in ultrathin Au nanowires, *Nano Lett.*, 2014, **14**, 4859–4866.

21 S. Xu, P. F. Li and Y. Lu, *In situ* atomic-scale analysis of Rayleigh instability in ultrathin gold nanowires, *Nano Res.*, 2018, **11**, 625–632.

22 Y. Chen, S. Milenkovic and A. W. Hassel, Thermal stability of {110} facet terminated gold nanobelts, *Appl. Surf. Sci.*, 2012, **258**, 6224–6231.

23 Z. X. Fan, M. Bosman, X. Huang, P. D. Yang, H. Zhang, *et al.*, Stabilization of 4H hexagonal phase in gold nanoribbons, *Nat. Commun.*, 2015, **6**, 7684.

24 Z. X. Fan, X. Zhang, J. Yang, X. J. Wu, H. Zhang, *et al.*, Synthesis of 4H/fcc-Au@Metal sulfide core–shell nanoribbons, *J. Am. Chem. Soc.*, 2015, **137**, 10910–10913.

25 Z. X. Fan, Z. M. Luo, X. Huang, B. Li, H. Zhang, *et al.*, Synthesis of 4H/fcc noble multimetallic nanoribbons for electrocatalytic hydrogen evolution reaction, *J. Am. Chem. Soc.*, 2016, **138**, 1414–1419.

26 P. F. Li, Y. Han, J. Song, H. Zhang, Y. Lu, *et al.*, Thermal effect and Rayleigh instability of ultrathin 4H hexagonal gold nanoribbons, *Matter*, 2020, **2**, 658–665.

27 P. F. Li, Q. L. Liao, Z. Zhang, Z. Z. Wang, Y. Zhang, *et al.*, Investigation on the mechanism of nanodamage and nanofailure for single ZnO nanowires under an electric field, *ACS Appl. Mater. Interfaces*, 2014, **6**, 2344–2349.

28 T. H. Yang and D. Qin, Capturing the equilibration pathway of nanomaterials metastable in both crystal structure and morphology, *Matter*, 2020, **2**, 519–525.

